Modeling and Testing of a Morphing Wing in Open-Loop Architecture

Andrei Vladimir Popov,* Teodor Lucian Grigorie,† and Ruxandra Mihaela Botez‡
École de Technologie Supérieure, Montreal, Quebec H3C 1K3, Canada
and
Youssef Mébarki§ and Mahmoud Mamou¶
National Research Council, Ottawa, Ontario K1A 0R6, Canada

This paper presents the modeling and experimental testing of the aerodynamic performance of a morphing wing in open-loop architecture. We show the method used to acquire the pressure data from the external surface of the flexible wing skin, using incorporated Kulite pressure sensors and the instrumentation of the morphing controller. The acquired pressure data are analyzed through fast Fourier transforms to detect the magnitude of the noise in the surface airflow. Subsequently, the data are filtered by means of high-pass filters and processed by calculating the root mean square of the signal to obtain a plot diagram of the noise in the airflow. This signal processing is necessary to remove the inherent noise electronically induced from the Tollmien–Schlichting waves, which are responsible for triggering the transition from laminar to turbulent flow. The flexible skin is required to morph the shape of the airfoil through two actuation points to achieve an optimized airfoil shape based on the theoretical flow conditions similar to those tested in the wind tunnel. Two shape memory alloy actuators with a nonlinear behavior drive the displacement of the two control points of the flexible skin toward the optimized airfoil shape. Each of the shape memory actuators is activated by a power supply unit and controlled using the Simulink/MATLAB® software through a self-tuning fuzzy controller. The methodology and the results obtained during the wind-tunnel test proved that the concept and validity of the system in real time are discussed in this paper. Real-time acquisition and signal processing of pressure data are needed for further development of the closed-loop controller to obtain a fully automatic morphing wing system.

I. Introduction

TO RESPOND to the ever-present need to reduce fuel and direct operating costs associated with new generations of aircraft, extensive research is underway to assess the performance of morphing wing technologies and concepts. These technologies will make it possible to enhance the aerodynamic performance of aircraft and to allow them to operate adaptively under a wide range of flight conditions. Moreover, the morphing technologies will be used to improve aircraft performance, expand the flight envelope, replace conventional control surfaces, reduce drag to improve range [1], and reduce vibrations and flutter [2]. Fly-by-wire and active control technology can also be used to achieve even more benefits in terms of direct operating cost reduction. In the near future, morphing vehicle technology will likely focus on small unmanned aerial vehicles (UAVs) [3]. Extremely complex, the interactions between aerodynamics, structures, controls, actuator power requirements, sensor integrations, and all other components are studied as part of the multi-

disciplinary research on morphing wing projects. Active control systems provide benefits in terms of reduced fuel consumption for morphing [4] and fly-by-wire aircraft. Their implementation requires knowledge of aeroservoelasticity interactions (interactions between unsteady aerodynamics, structure, and controls). In the Mission Adaptive Wings research program [4], the aerodynamic benefits of smooth variable camber and automatic flight control modes were determined for the following systems: maneuver camber control, cruise camber control, maneuver enhancement/gust alleviation, and maneuver load control.

Shape memory alloys (SMAs) used in morphing flap actuation were developed in ultralight and scaled models made of balsa wood and nylon sticks, due to the favorable characteristics of high strength and low weight. The SMA actuators were controlled using robust nonlinear controllers [5,6]. Wind-tunnel studies were performed on morphing wing flap prototypes using SMA wires (NiTiNol). The trailing edge was morphed by means of six NiTiNol wires that could pull the flap assembly upon electrical activation, while ten springs acted to regain the initial wing configuration when the SMA wires cooled down.** Another morphing flap actuated using SMAs was developed, using four SMA wires anchored in four different chord points. A wing prototype with flexible skin made of a fiberglass composite and a rubber sheet was manufactured and tested [7].

Torsion bars and wires using SMA (NiTiNol) for the roll control of a morphing wing model aircraft were tested in wind tunnel and during flight [8]. The "hingeless wing" concept using SMA wires was investigated [9,10].

In the present paper, we perform the conceptual design and validation of an active control system for the transition flow control of a wing model in wind-tunnel tests. Various proportional–integral–derivative (PID) based methods were studied to produce the controller for the laminar-to-turbulent transition flow control [11].

*Ph.D. Student, Laboratory of Active Controls, Aeroservoelasticity and Avionics, Department of Automated Production Engineering, 1100 Notre Dame Street West; andrei-vladimir.popov.@ens.etsmtl.ca. Member AIAA.

†Postdoctoral Fellow, Laboratory of Active Controls, Aeroservoelasticity and Avionics, Department of Automated Production Engineering, 1100 Notre Dame Street West; ltgrigorie@yahoo.com. Member AIAA.

‡Professor, Laboratory of Active Controls, Aeroservoelasticity and Avionics, Department of Automated Production Engineering, 1100 Notre Dame Street West; ruxandra@gpa.etsmtl.ca. Member AIAA.

§Research Officer, Institute for Aerospace Research, Uplands Building U66, Montreal Road. Member AIAA.

¶Research Officer, Institute for Aerospace Research, Uplands Building U66, Montreal Road. Member AIAA.

**Data about "Morphing Wing Design Using NiTiNol Wire," by J. C. Benavides and G. Correa (Missouri Univ. of Science and Technology, Intelligent System Center) available online at http://isc.mst.edu/reu/2004indprojects/2004-6.html [retrieved 5 March 2010].
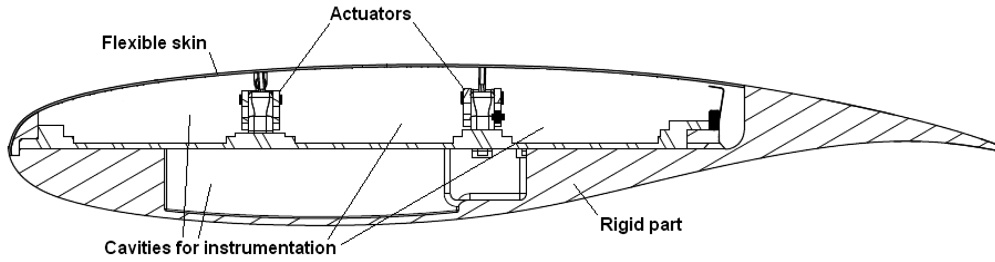
Fig. 1   Cross section of the morphing wing model.

Simulations and experimental multidisciplinary studies were performed through wind-tunnel measurements for a morphing wing equipped with a flexible skin, smart material actuator SMAs, and different types of pressure sensors. The aim of these studies is to move the transition point from laminar to turbulent flow closer to the trailing edge by use of a controller to obtain a larger laminar flow region.

A hardware system, which deforms the airfoil to its optimized shape to allow long laminar runs, was designed and manufactured [12]. This research project studies the possibility of the technological realization of a morphing wing followed by validation in a wind-tunnel environment, the possibility of detecting small pressure variations in the airflow boundary layer, and the processing and analyzing the acquired signals in real time.

The configuration of the morphing wing wind-tunnel model consists of a rectangular wing model that incorporates two parts: one rigid part built with a metal (aluminum alloy) designed to sustain all the aerodynamic and actuators loads, and one flexible part consisting of a flexible skin installed on the upper surface of the rigid wing part; see Fig. 1. As a reference airfoil, the natural laminar flow airfoil, wind-tunnel experimental airfoil, was chosen. Its aerodynamic performance was investigated at the Institute for Aerospace Research, National Research Council Canada (IAR–NRC) in the transonic regime in [13]. Thirty-five flight conditions were studied during wind-tunnel tests: seven values for the angle of attack, which varied between −1 and 2 deg, and five Mach number values within the range of $M[0.2, 0.3]$. For these flight conditions, 35 optimized airfoils were obtained for the airflow case combinations of Mach numbers and angles of attack; see Table 1. The optimized airfoils were calculated by modifying the reference airfoil for each airflow condition as combinations of angles of attack and Mach numbers. The optimized airfoil shapes were realized using an optimizing routine that varied the vertical position of each actuator. The optimizing routine was coupled with a spline curve model of the flexible skin and the XFoil computational fluid dynamics (CFD) code, and then the first generation of optimized airfoils, C1XX, was obtained; see Table 1 [14]. The XFoil CFD code is free licensed software in which the e^n transition criterion is used, and which was presented in [15,16]. The imposed conditions of the first optimization were expressed in terms of the transition point position displacement as near as possible to the airfoil trailing edge, while maintaining a constant lift.

The flexible skin was required to change the shape of the airfoil through two actuation points to realize an optimized airfoil for a given airflow condition under which the test was performed. Two rows of shape memory alloy actuators with a nonlinear behavior drove the displacement of the two control points on the flexible skin

to obtain the optimized airfoil shape [17]. Each of the shape memory actuators was activated by a power supply and controlled using Simulink/MATLAB® through an in-house designed controller. For different flight conditions (angles of attack α and Reynolds number Re), the controller received the values of the actuator displacements stored in a database, while the airfoil upper surface pressure coefficient distribution C_p determined from the surface pressure measured by the sensors was visualized in real time during wind-tunnel tests. The C_p distribution recorded with the pressure sensors was compared with a CFD database, which was generated using the XFoil software.

In this paper, the methods used to acquire pressure data from the external surface of the flexible skin wing by means of Kulite sensors and by the instrumentation of the morphing controller are shown. The Tollmien–Schlichting waves that determine the laminar-to-turbulent transition were detected and investigated using microphones and hot films sensors in [18,19]. These studies were essential in reaching decisions concerning the minimal technical specifications for sensors that could be used in these applications. In our research, we tested two types of pressure sensors, optical and Kulite. The tests performed in the wind tunnel showed that the optical sensors were not accurate enough to detect the small pressure variations at the high sampling rate that would allow detection of the Tollmien–Schlichting waves. The acquired pressure data were analyzed through fast Fourier transforms (FFT) to detect the pressure signal spectra. Subsequently, the data were run through high-pass filters and processed by calculating the rms of the signal to a plot diagram of noise quantity in the airflow. This real-time computing process was necessary to locate the sensor that had the highest amplitude of the Tollmien–Schlichting waves, which indicate the laminar-to-turbulent flow transition.

II.   Experimental Setup

From the initial studies related to the optimal configuration of the flexible structure [14,17], it can be concluded that the structure was conveniently designed to be operated by two actuation lines positioned at 25.3 and 47.6%, respectively, of the chord from the leading edge of the airfoil; see Fig. 1.

For this configuration, the aerodynamic forces coupled with the actuators can get the flexible skin to the position of maximum deflection, while the gas springs remind the SMA to return the flexible structure to its nominal position.

Under the aerodynamic loads for a given optimized airfoil shape and flight condition, the SMA actuation system would produce sufficient force and displacement at the actuation line level. The vertical displacements induced by the two SMA actuators at the two

Table 1   Test flow conditions for 35 wing airfoils

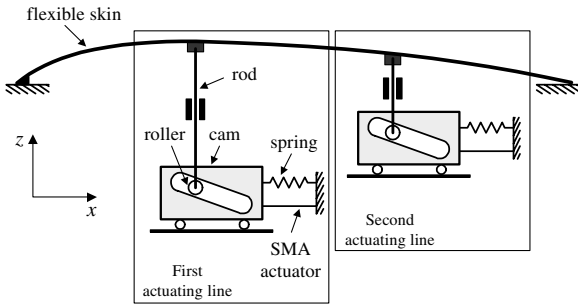| Mach	Re ($\times 10^6$)	Angle of attack, deg						
		−1.00	−0.50	0.00	0.50	1.00	1.50	2.00
0.200	2.29	C101	C102	C103	C104	C105	C106	C107
0.225	2.56	C108	C109	C110	C111	C112	C113	C114
0.250	2.83	C115	C116	C117	C118	C119	C120	C121
0.275	3.10	C122	C123	C124	C125	C126	C127	C128
0.300	3.36	C129	C130	C131	C132	C133	C134	C135

Fig. 2 Schematics of the actuating system with SMAs.

actuation points are denoted by dY_1 and dY_2, respectively. Scheme of the instrumented wing configuration are given in Figs. 2 and 3.

Each actuating line of the system contains a cam, which moves in translation relative to the structure (in the x-axis direction in Fig. 2). The cam causes the movement of a rod linked to a roller and on the skin (in the z-axis direction) [17]. The initial position of the roller is restored by the compression gas spring. When the SMA is heated, the actuator contracts and the cam moves to the right, resulting in the rise of the roller and an upward vertical displacement of the skin. In contrast, the cooling of the SMA results in a movement of the cam to the left and, thus, a downward displacement of the skin; see Fig. 2.

The architecture of the open-loop control system of the wing model, the SMA actuators, and the controller are shown in Fig. 3. The two actuators have six SMA wires that are individually powered by two AMREL SPS power supplies, controlled through analog signals by a Quanser Q8 control board, which was programmed through Simulink/xPC. In Simulink, a user interface was implemented, allowing the user to choose the optimized airfoil shapes and to provide the necessary values for the SMA displacements, dY_1 and dY_2.

Each SMA actuator has its own controller that maintains the actuator in the desired position. The tested controller concept involves a self-tuning fuzzy controller. Furthermore, a classical PID controller was tested as well. The controllers act on the electrical current, which heats the SMA to allow it to change its length.

The initial input, which is the optimized airfoil for any flow condition, is chosen manually by the operator from the computer database through a user interface. Next, the displacements (dY_1 and dY_2) that need to be reproduced by the two control points on the flexible skin are sent to the controller. This controller sends an analog 0–2 V signal to the power supply, which provides a continuous current of 0–20 A/20 V to the SMA. The SMA responds accordingly and changes its length according to the temperature of the wire. This results in the actuators changing positions, and the position of the actuator is recorded by a linear variable differential transducer (LVDT). The signal position received from the LVDT is compared to the desired position, and the error obtained is fed back to the controller. If the realized position is greater than the desired position, the controller disconnects the control current, letting the SMA wire cool down. During the cooling down process, the SMA maintains its length due to the hysteretic behavior, and this effect is taken into account for actuator displacement. Moreover, the controller uses three thermocouples signals from each SMA wire to monitor the temperature of the wires and maintains it below 130°C, which is the upper limit.

The pressure data acquisition was performed using 15 Kulite pressure sensors and a NI-DAQ USB 6210 card with 16 analog inputs (Fig. 3), at a total sampling rate of 250 k samples/s. The input channels were connected directly to the IAR–NRC analog data acquisition system, which in turn was connected directly to the 15 Kulite sensors. One extra channel was used for wind-tunnel dynamic pressure acquisition to calculate the pressure coefficient C_p from the pressure mean values measured by the 15 sensors. The sampling rate of each channel was 15 k samples/s, which allowed a boundary-layer pressure fluctuation FFT spectral decomposition of up to 7.5 kHz for all channels. The signal was processed using Simulink, high-pass filtered at 1 kHz, and displayed the mean value, the rms value, and the spectra for each pressure signal channel in real time.
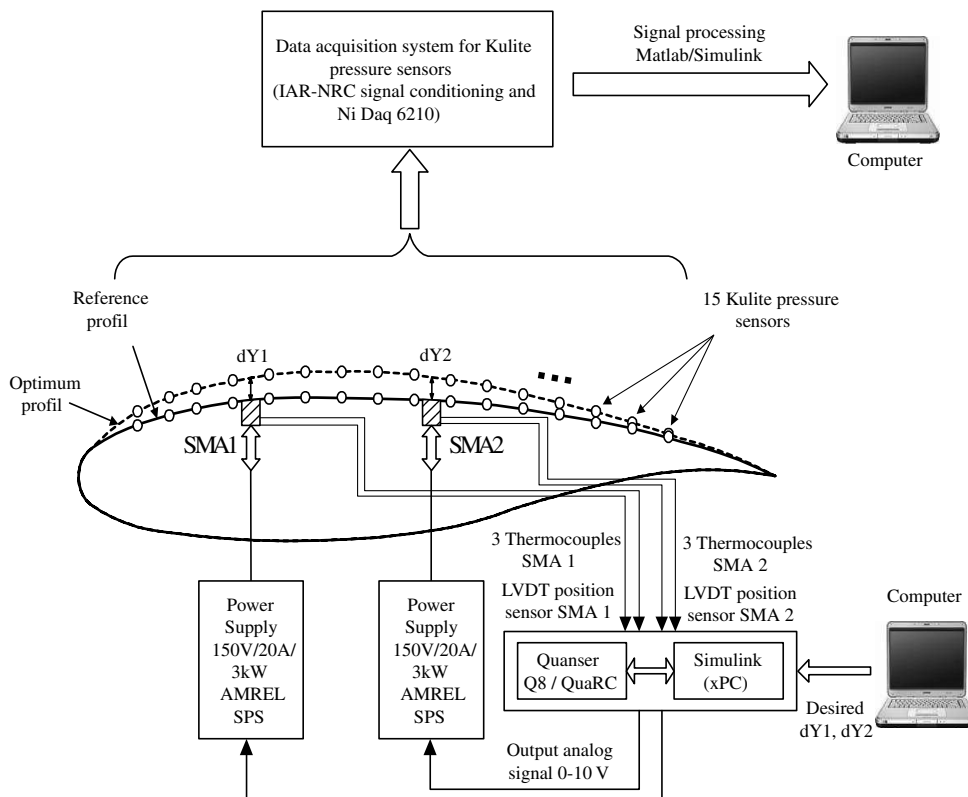

Fig. 3 SMA control architecture and sensor acquisition systems of the morphing wing model.

III.   Results of Wind-Tunnel Tests

The following proposed milestones were achieved during the wind-tunnel tests performed at IAR–NRC:

1) SMA open-loop control testing used a self-tuning fuzzy controller and a PID controller.

2) Real-time pressure signal acquisition and processing tests used signal filtering, FFT spectral decomposition, rms calculation, and

detection of the transition location, necessary for further development of a closed-loop controller to obtain a fully automatic morphing wing system.

3) Graphic user interface (GUI) was tested by keeping the dialog between the MATLAB work space and the Simulink schemes that were running in real time.

From the self-tuning fuzzy versus PID open-loop control analysis, it was found that, due to its in-built optimization algorithm, the
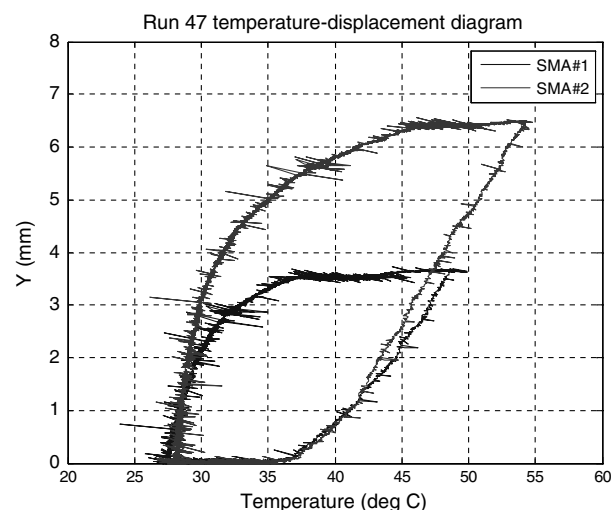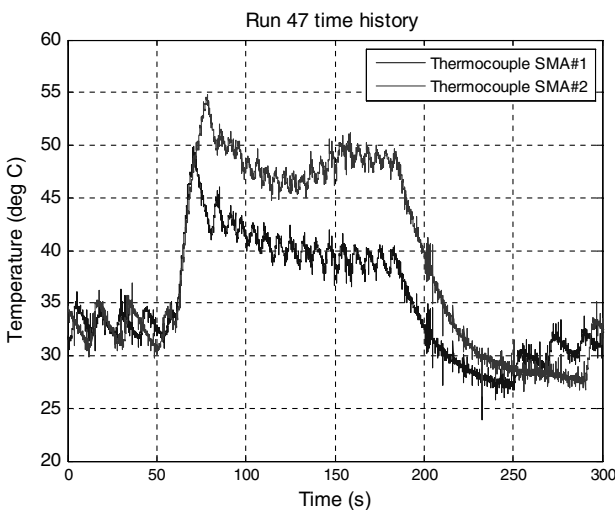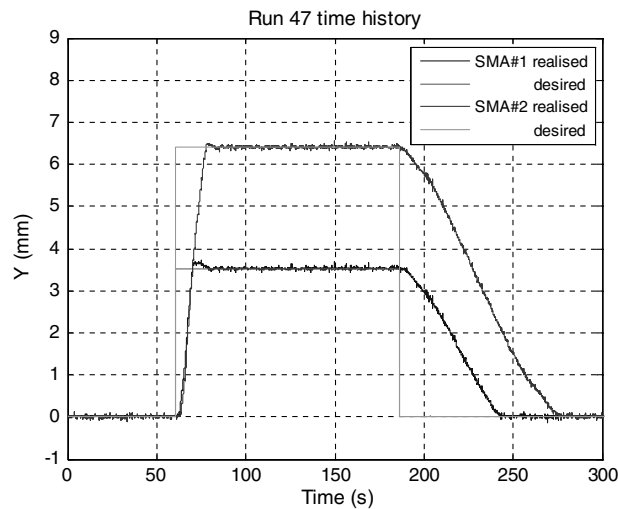

Fig. 4   PID controller results for run 47 at Mach = 0.227 and α = 0 deg.

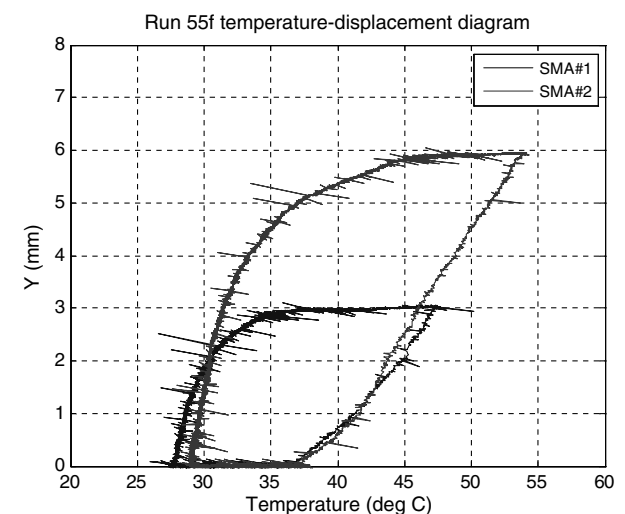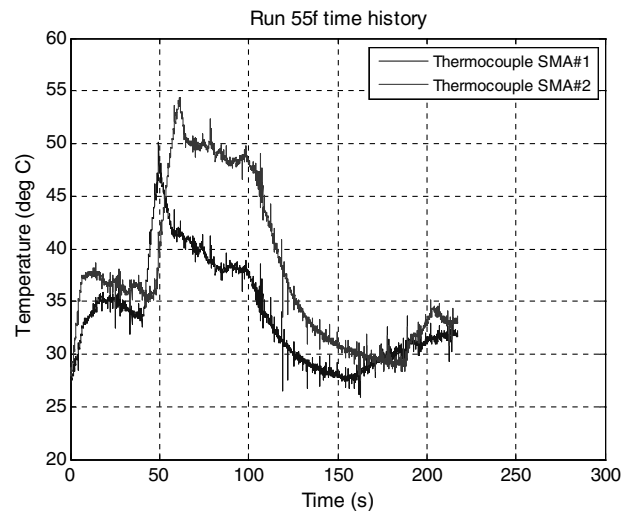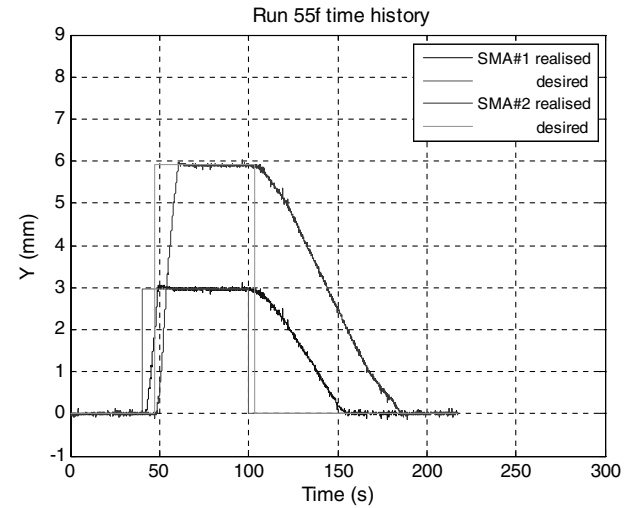**Fig. 5   Self-tuning fuzzy controller results for run 55 at Mach = 0.3 and α = 1 deg.**

self-tuning fuzzy controller had a smoother control than the PID controller for the same displacements. The PID controller used a switch that connected and disconnected the power sources supplying the SMA with 10 A when heating was needed and 0 A when cooling was needed, which had as a consequence the saw teeth behavior in the temperature–time-history plot, as shown in Fig. 4. The fuzzy controller kept a narrow control over the temperature variations in the SMA wires due to the fuzzy algorithm that produced the needed value of current in the interval of 0–10 A, without going to the extremes of maximum or minimum current; the smooth control of the SMA heating is shown in Fig. 5b. The third plot of Figs. 4c and 5c shows the temperature-displacement hysteresis behavior of the SMA wires, which explains the temperatures needed by SMA to achieve the desired displacements.

Figures 6 and 7 show the screen shots of the GUI used to control the system during the wind-tunnel tests. These figures show the plots of the C_p, rms, and power spectra for the pressure signals channels recorded during the wind-tunnel tests. The signals of sensors 11 and 12 were removed from the plots owing to their faulty dynamical signals, so that only 13 signals are plotted in Figs. 6 and 7. Sensor 5 had a leak in the pressure reference tubes that lead to a faulty value of the C_p values. On the other hand, the dynamic signal for sensor 5 was good, and as such, its value was retained in the plots.

The "CHARGE" push button runs a function that uses XFoil to calculate the C_p and N factor distribution over the upper surface of the reference airfoil and morphed airfoil in the aerodynamic conditions of the case number, such as "C129." The two airfoils (reference and optimized) are selected from the database and plotted starting from their leading edge (x coordinate $= 0$ mm) to the end of the flexible skin (x coordinate $= 380$ mm). The lower curve belongs to the reference airfoil, and the upper curve belongs to the optimized (morphed) airfoil.

In these graphs, the C_p values calculated by XFoil for various sensors are defined by circles; the lower C_p distribution corresponds to the reference airfoil, and the upper C_p distribution corresponds to the optimized airfoil. In the lower figure, the N factor calculated with XFoil for both airfoils are plotted using the same symbols as the above plots. The critical value $N_{cr} = 7.34$ was used in the simulation to match the turbulence level $T = 0.14\%$ measured in the wind tunnel using Mack's correlation [20] and the plotted values on the figure were normalized (N/N_{cr}):

$$N_{cr} = -8.43 - 2.4 \cdot \log(T) \tag{1}$$

In Figs. 6 and 7, the predicted transition position calculated by XFoil in the reference airfoil case was found to be the tenth position of the available sensor positions, which corresponded to 0.45 x/c, and the predicted transition calculated by XFoil in the optimized airfoil case was found to be the thirteenth position of the available sensor positions, which corresponded to 0.67 x/c.

In the upper right corner of the left-hand side plots, three sets of actuator displacement values dY_1 and dY_2 are shown in three columns: the first column, the values requested by the user are transferred to the Simulink program by pressing the "Request" button; the second column displays the optimized values automatically calculated from the difference between the database's optimized airfoil and reference airfoil values (these values are sent to the Simulink program by pressing the "Optim" button); the third column displays the real-time displacement values received from the actuator position sensors through the acquisition card. In the right corner of the GUI figure is a set of push buttons that allow the user to control the running of the Simulink program.

The lower right corner of the GUI figure shows the number of the sensor located at the transition position calculated with XFoil for the reference airfoil (up), the number of the sensor located at the transition position calculated with XFoil for the optimized airfoil (middle), and the number of the sensor with the maximum noise level (maximum rms of the filtered signal) that corresponds to the real transition position (down).

The power spectra plots on the right side of Figs. 6 and 7 show the 13 channels as follows: the first five channels are shown in the upper figure named "Ch 1–5," the next five channels are shown in the middle figure named "Ch 6–10," and the next five channels, which are actually three because two of them were removed, are shown in the lower figure named "Ch 11–15."

For each aerodynamic condition during the wind-tunnel tests, the pressures were recorded when the wing had a reference airfoil (actuators on zero), then the pressures were recorded again when the
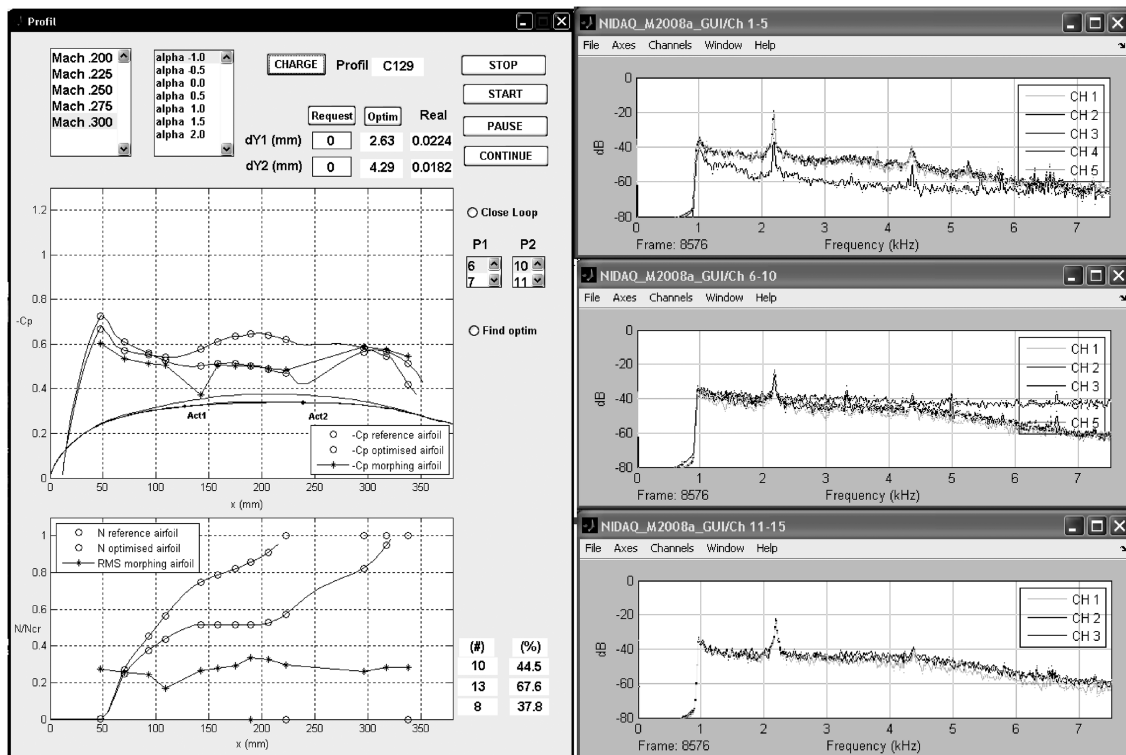

Fig. 6   Airflow case C129, Mach number $= 0.3$, $\alpha = -1$ deg, reference (original) airfoil.
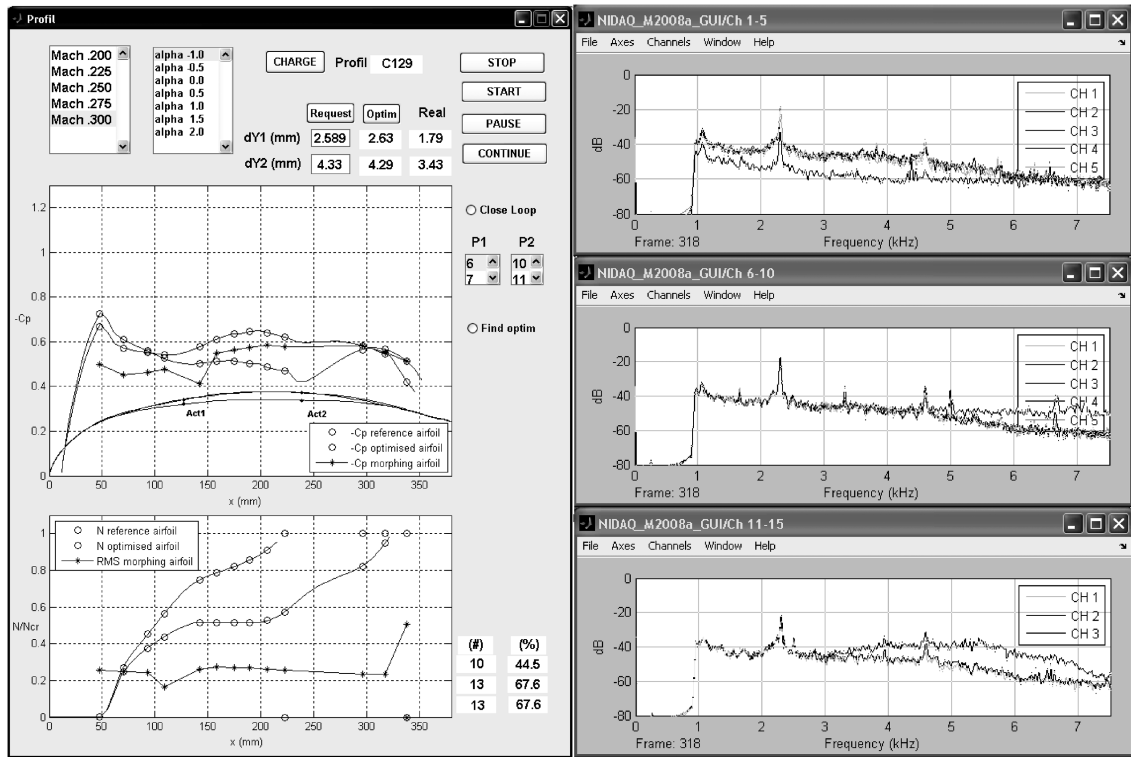
Fig. 7   Airflow case C129, $M = 0.3$, $\alpha = -1$ deg, optimized (morphed) airfoil.

wing was morphed to the optimized airfoil (actuators deployed). Figure 6 shows the pressures recorded during the reference phase, and Fig. 7 shows the pressures recorded during morphed phase.

In the reference airfoil case (Fig. 6), the mean values of the recorded pressure signal from the Kulite sensors were displayed in the same plot with the values calculated by XFoil in real time, showing a good match. The rms plot, displayed in the GUI figure with star symbols, showed the quantity of the noise for each pressure signal in real time, and was normalized and displayed in the same plot with the normalized N factor plot. The sensor with the maximum rms, the eighth sensor plotted, which was located at $0.38\ x/c$,

indicated the Tollmien–Schlihting wave's occurrence, which is the transition indication [18,19]. The spectral decomposition of the pressure signals confirmed the Tollmien–Schlichting wave's occurrence in the eighth sensor, visible in the highest power spectra (the third channel in the middle right-hand side plots) in the frequency band of 3–7.5 kHz.

In the morphed-to-optimized airfoil case (Fig. 7), the rms plot, displayed in the GUI figure with star symbols, showed that the sensor with the maximum rms became the thirteenth sensor plotted, which was located at $0.67\ x/c$. The spectral decomposition of the pressure signals confirmed the Tollmien–Schlichting wave's occurrence in the
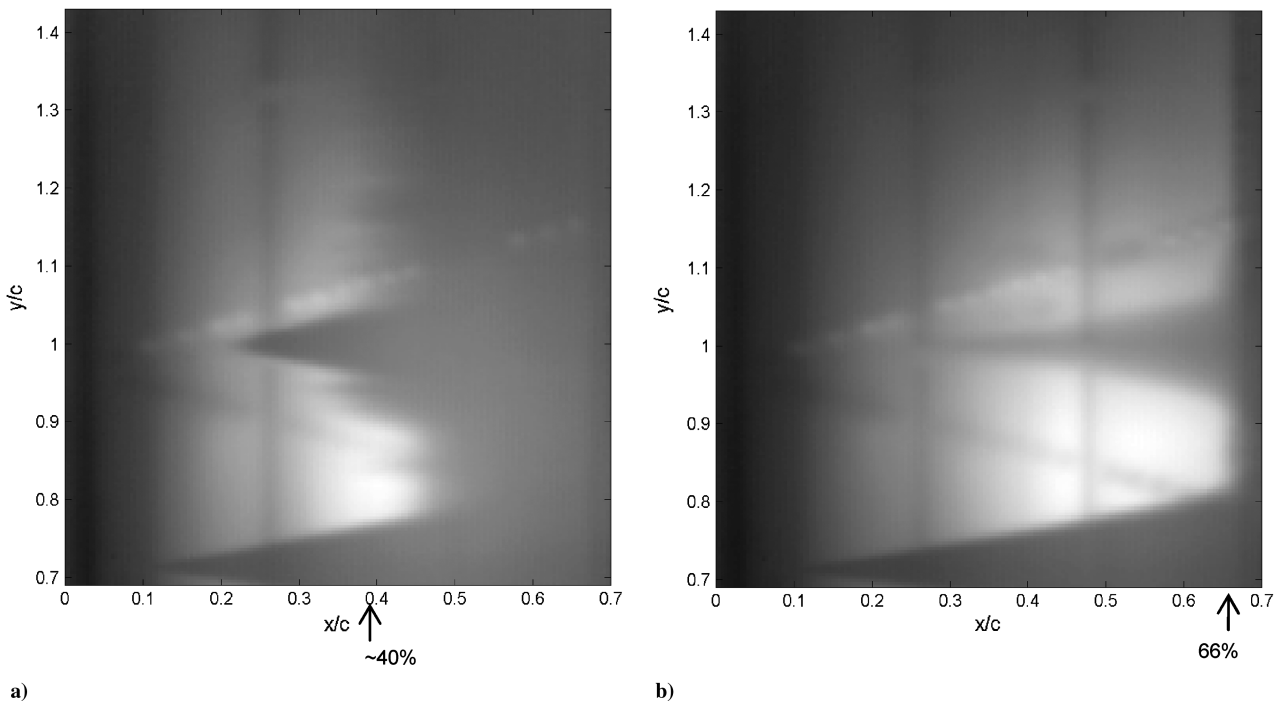

Fig. 8   Infrared images at $M = 0.3$ and $\alpha = -1$ deg: a) reference airfoil, and b) optimized airfoil C129.

thirteenth sensor, visible in the highest power spectra (the third channel in the lower right-hand side plots) in the frequency band of 3–7.5 kHz.

In support of the discrete pressure instrumentation, infrared thermography (IR) visualization was performed to detect the transition location on the upper surface of the morphing wing and to validate the pressure sensor analysis. The transition detection method using IR is based on the differences in the laminar and turbulent convective heat transfer coefficient and was exacerbated by the artificial increase of model-airflow temperature differences. In the resulting images, the sharp temperature gradient separating high-temperature (white intensity in image) and low-temperature (dark intensity) regions indicates the transition location.

Figure 8 displays the region of the morphing wing measured by the IR camera between $0 < x/c < 0.7$ and $0.7 < y/c < 1.4$. Flow is from left to right. The aft rigid portion of the wing, made of aluminum, was not considered in the IR measurements. The two rows of pressure sensors positioned in a V shape and the locations of the SMA actuators as two vertical stripes were visible in the IR images. The upper row of sensors is the Kulite sensors' thermal signature and the lower row of sensors is the optical sensors' thermal signature on the IR image.

Figures 8a and 8b show the IR transition images obtained for $M = 0.3$ and $\alpha = -1$ deg in the reference and optimized configurations, respectively. The transition, originally located at approximately $x/c = 0.40$ in the Kulite sensors' row and shown with an arrow in Fig. 8a, has been moved to $x/c = 0.66$, shown with an arrow in Fig. 8b for the morphed wing configuration (case C129). The optimization has significantly extended the laminarity of the flow over the upper wing surface, as determined by the Kulite sensors. The airfoil shape optimization has also improved the apparent two dimensionality of the flow: the transition appears vertical in the optimized morphed case (Fig. 8b), except for the turbulent wedges triggered by the leak of Kulite sensor 5 (at $x/c = 0.2$ and $y/c = 1$). These results, which are in agreement with the Kulite sensors' recorded data, confirm the use of discrete transducers as control parameters for wing shape optimization.

IV. Conclusions

The paper presented wind-tunnel experimental testing of a morphing wing in an open-loop architecture. The method used for acquiring the pressure data from the external surface of the flexible skin wing by means of Kulite pressure sensors and the instrumentation of the morphing controller were shown. The realized tests showed that the SMA actuators performed well, with temperatures of lower than 60°C under maximal deployment without interfering with the electric systems of the Kulite sensors. Moreover, the wind-tunnel tests validated the PID and self-tuning controller architecture for open-loop operation, and allowed the real-time visualization of the transition by means of the spectral decomposition and rms calculation of the pressure signal received from Kulite sensors, which were able to detect the unsteady pressure variations during wing testing with the reference and morphed airfoil in the wind tunnel.

Acknowledgments

References

[1] Zingg, D. W., Diosady, L., and Billing, L., "Adaptive Airfoils for Drag Reduction at Transonic Speeds," AIAA Paper 2006-3656, 2006.

[2] Rodriguez, A. R., "Morphing Aircraft Technology Survey," AIAA Paper 2007-1258, 2007.

[3] Livne, E., "Future of Airplane Aeroelasticity," *Journal of Aircraft*, Vol. 40, No. 6, 2003, pp. 1066–1092.
doi:10.2514/2.7218

[4] Moorhouse, D., Sanders, B., von Spakovsky, M., and Butt, J., "Benefits and Design Challenges of Adaptive Structures for Morphing Aircraft," *The Aeronautical Journal*, 2006, Vol. 110, No. 1105, pp. 157–162.

[5] Alasty, A., Alemohammad, S. H., Khiabani, R. H., and Khalighi, Y., "Maneuverability Improvement for an Ultra Light Airplane Model Using Variable Shape Wing," AIAA Paper 2004-4831, 2004.

[6] Song, G., and Ma, N., "Robust Control of a Shape Memory Alloy Wire Actuated Flap," *Smart Materials and Structures*, Vol. 16, 2007, pp. N51–N57.
doi:10.1088/0964-1726/16/6/N02

[7] Seow, A. K., Liu, Y., and Yeo, W. K., "Shape Memory Alloy as Actuator to Deflect a Wing Flap," AIAA Paper 2008-1704, April 2008.

[8] Mason, H. W., Robertshaw, H., and Inman, D. J., "Recent Experiments in Aerospace and Design Engineering Education," AIAA Paper 2004-0415, Jan. 2004.

[9] Barbarino, S., Pecora, R., Lecce, L., Concilio, A., Ameduri, S., and Calvi, E., "A Novel SMA-Based Concept for Airfoil Structural Morphing," *Journal of Materials Engineering and Performance*, Vol. 18, No. 5, 2009, pp. 696–705.
doi:10.1007/s11665-009-9356-3

[10] Mirone, G., "Design and Demonstrators Testing of Adaptive Airfoils and Hingeless Wings Actuated by Shape Memory Alloy Wires," *Smart Structures and Systems*, Vol. 3, No. 1, 2007, pp. 89–114.

[11] Popov. A-V., Labib, M., Fays, J., and Botez, R. M., "Closed Loop Control Simulations on a Morphing Laminar Airfoil Using Shape Memory Alloys Actuators," *Journal of Aircraft*, Vol. 45, No. 5, 2008, pp. 1794–1803.
doi:10.2514/1.37073

[12] Coutu, D., Brailovski, V., and Terriault, P., "Promising Benefits of an Active-Extrados Morphing Laminar Wing," *Journal of Aircraft*, Vol. 46, No. 2, 2009, pp. 730–731.
doi:10.2514/1.40657

[13] Khalid, M., "Navier–Stokes Investigation of Blunt Trailing Edge Airfoils Using O-Grids," *Journal of Aircraft*, Vol. 30, No. 5, 1993, pp. 797–800.
doi:10.2514/3.46416

[14] Sainmont, C., Paraschivoiu, I., and Coutu, D., "Multidisciplinary Approach for the Optimization of a Laminar Airfoil Equipped with a Morphing Upper Surface," NATO AVT-168 Symposium on Morphing Vehicles, 2009.

[15] Drela, M., "Implicit Implementation of the Full e^n Transition Criterion," AIAA Paper 2003-4066, 2003.

[16] Drela, M., and Giles, M. B., "Viscous-Inviscid Analysis of Transonic and Low Reynolds Number Airfoils," *Journal of Aircraft*, Vol. 25, No. 10, 1987, pp. 1347–1355.
doi:10.2514/3.9789

[17] Georges, T., Brailovski, V., Morellon, E., Coutu, D., and Terriault, P., "Design of Shape Memory Alloy Actuators for Morphing Laminar Wing with Flexible Extrados," *Journal of Mechanical Design*, Vol. 131, No. 9, 2009, pp. 091006-1–091006-9.
doi:10.1115/1.3160310

[18] Nitcshe, W., Mirow, P., and Dorfler, T., "Investigations on Flow Instabilities on Airfoils by Means of Piezofoil-Arrays," *Laminar-Turbulent Transition IUTAM Symposium*, Springer–Verlag, Berlin Heidelberg, Sept. 1990, pp. 129–135.

[19] Mangalam, S. M., "Real-Time Extraction of Hydrodynamic Flow Characteristics Using Surface Signature," *IEEE Journal of Oceanic Engineering*, Vol. 29, No. 3, 2004, pp. 622–630.
doi:10.1109/JOE.2004.833098

[20] Mack, L. M., *Transition and Laminar Instability*, Jet Propulsion Lab,, Publication 77-15, Pasadena, CA, 1977.